Acta Polytechnica **63**(6):439–450, 2023
https://doi.org/10.14311/AP.2023.63.0439

Published by the Czech Technical University in Prague

SEMI-ANALYTICAL APPROACH-BASED STUDIES OF THE SQUEEZE FILM LUBRICATION BETWEEN ROUGH POROUS ANNULAR DISCS: RABINOWITSCH FLUID MODEL

Amit Kumar Rahul[a,*], Manoj Kumar Singh[a], Ravi Tiwari[b], Sourabh Paul[b], Pentyala Srinivasa Rao[c], Rohahn Biswas[d]

[a] *Vellore Institute of Technology, School of Advanced Sciences (SAS), Division of Mathematics, Chennai 600127, Tamil Nadu, India*

[b] *Vellore Institute of Technology, School of Electronics Engineering (SENSE), Chennai 600127, Tamil Nadu, India*

[c] *Indian Institute of Technology, Department of Mathematics & Computing, Dhanbad, 826004, India*

[d] *Vellore Institute of Technology, School of Electrical Engineering (SELECT), Chennai 600127, Tamil Nadu, India*

[*] corresponding author: akrahulism@gmail.com

Abstract. In recent years, there has been much interest in the effects of porosity and surface roughness (SR) or geometric irregularities between two moving plates under hydrodynamic lubrication. Porous bearings are used extensively in wide range of equipment, including computers, office equipment, home appliances, electric motors, and vehicles. In light of the importance of the aforementioned applications, we explored how SR and porous materials affect annular discs under the condition of a squeeze film. A five-point Gauss quadrature integral formula has been used to examine the characteristics of annular discs and a small perturbation method has been used to discretise the governing Rabinowitsch fluid flow (RFF) equations. The impact of nonlinear parameters on the behaviour of porosity and SR have been visualised in terms of film pressure (FP), load carrying capacity (LCC), and squeeze response time (SRT) of annular discs. Under the conditions of pseudoplastic and dilatant fluids, the effects of SR and porous materials between annular discs have been estimated in the form of the film pressure, LCC, and SRT and are presented in this manuscript as tables and graphs. According to the findings, the performance of an annular disc is significantly affected by porous material and radial roughness patterns. In addition, when RFF is carried through a rough surface and porous media, the performance is found to improve for dilatant fluids but suffer for pseudoplastic fluids.

Keywords: Annular discs, squeeze film, Rabinowitsch fluid model, surface roughness, porous wall.

1. Introduction

Squeeze film (SF) is used in a variety of applications, such as turbomachinery, disc clutches, and viscous-lock systems. Recently, there has been a significant increase in interest in this area. The performance of annular plates under SF has been studied under Newtonian fluids (NF) and non-Newtonian fluids (NNF) by Allen and McKillop [1], and Naduvinamani et al. [2]. It has been discovered that squeeze film (SF) increases the efficiency and reliability of bearings while also prolonging their lifespan. The NF is a broad term for the linear relationship between shear strain and the rate of change. Experimental research has shown that novel fluids can be constructed from an NF to include some additional components that behave as an NNF. They consist of high-molecular-weight polymers, viscosity index improvers, polyisobutylene, etc. (Spike [3]).

The non-Newtonian fluids (NNF) have a non-linear relationship with both the rate of shear strain and the shear stress. Different NNF models, such as the power-law fluid model, Rabinowitsch fluid model (RFM), and couple-stress fluid model, have been tested by a number of tribologists to investigate the performance of bearings. Lin and Hung [4] have investigated the performance of circular plates lubricated with a couple stress fluid model and a power-law fluid model by Wang et al. [5]. Several researchers have studied the demonstration of the RFM for different types of bearings. Wada and Hayashi [6, 7] were the first to study theoretically and experimentally the mechanism of journal bearing in the presence of pseudoplastic fluids. Furthermore, Lin [8] and Siddangouda et al. [9] investigated the performance of parallel annular discs and static characteristics of an inclined plane slider bearing under the condition of RFM. These studies suggest that under RFM the bearing performance is influenced by the characteristics of the dilatant fluids, whereas the pseudo-plastic behaviour results in a lower concentration of bearing stability compared to NF.

For five decades, permeable materials have been widely used in industry to improve bearing performance (Bujurke et al. [10], Morgan and Cameron [11]). With the use of Darcy's model, Morgan and Cameron [10] were the first researchers who inves-

tigated the porous effect on bearing surfaces. Patel et al. [12] have considered double-layer porous surface with a curved squeeze film. Bhat and Deheri [13] conducted a study on squeeze film behaviour in porous annular discs that are lubricated with magnetic fluid.

Recently, Walicka et al. [14], Rao and Rahul [15–17], and Rahul et al. [18] have applied the RFM on a curvilinear and SF bearing to study the characteristics of the dilatant fluid between the porous media. These researchers were concerned with how the porous wall affected the performance of the bearings. It was concluded that the Rabinowitsch fluid property, which exists in porous media, has a substantial impact on the bearings' characteristics and lengthens their lifespan.

The goal of many researchers is to show how SR affects the thin film lubrication bearing. The bearing performance, including pressure, load, friction, drags, and other factors, is influenced by this condition's surface roughness. Various methodologies have been introduced to examine the impact of SR on the performance of bearings. Christensen [19, 20] first established the stochastic theory of thin film lubrication of rough bearing surfaces. The combined effects of SR and porosity with MHD between annular discs have been taken into consideration by Baksh and Naganagowda [21]. By analysing the permeability influence on the rotor linear stability, D'Agostino et al. [22] examined the unstable oil film forces in porous bearings. Vashi et al. [23], have considered the Neuringer-Rosenzweig model to investigate the performance of circular stepped plates in the existence of couple stress, porosity, and SR Siddangouda et al. [24] investigated the combined impact of SR and viscosity change brought on by additives on long journal bearing. According to Munshi et al. [25], a rough porous sine film slider bearing with ferrofluid lubrication was subjected to a sinusoidal magnetic field.

Shimpi and Deheri [26] investigated the deformation effect of a magnetic fluid-based squeeze film in rough rotating curved porous annular plates. Patel et al. [27] investigated the lubrication of a rough porous hyperbolic slider bearing with slip velocity using ferrofluid. Patel and Deheri [28] studied the joint effect of slip velocity and roughness on the ferrofluid lubrication of a curved rough annular squeeze film using the Jenkins model. Vashi et al. [29] studied the longitudinally rough porous circular stepping plates based on the Neuringer-Roseinweig model in the presence of couple stress. The influence of a porous structure, slip velocity, and Rosensweig's viscosity on the ferrofluid-based squeeze film on porous curved annular plates was explored by Patel et al. [30]. Pressure generations in a rough conical bearing using non-Newtonian Rabinowitsch fluid with variable viscosity have been investigated by Rao and Rahul [31]. A hydrostatic conical bearing that is externally pressured and lubricated with RFM has been studied by Walicka et al. [32] for how wall porosity and surface roughness affect steady performance. Recently, Rahul and Rao [33, 34] investigated the behaviour of annular discs and circular stepping plates in the presence of a viscosity variable of Rabinowitsch fluid with a rough and porous surface. They have discussed that a one-dimensional azimuthal (Radial) roughness pattern on the rough porous circular plate increases (decreases) the load-carrying capacity and the squeeze film time as compared to the corresponding smooth case. Moreover, in circular stepped plates with the presence of the porous wall, the load capacity, and squeeze time decreases compared to non-porous case.

1.1. Research gap

The above researchers concluded that transverse roughness patterns on the bearing surface increase FP and LCC. Despite the much anticipated future of squeeze film bearings, not enough research has been done. The majority of the work has been performed without taking into account the impacts of porous discs, the Rabinowsitch fluid model, and surface roughness, according to the literature review. The following issues weren't covered in the papers that were previously published.

a) Analysis of the characteristics of a squeeze-film of annular discs using the RF model to determine the effectiveness of the porosity and surface roughness.

b) Investigation of the effect ω, H_0^*, R_0^*, c^* on the trend P^* for a constant Ω. Determining the influence of ω, H_0^*, R_0^*, c^* on the trend W^* for a constant h^* and Ω.

c) The impact of ω, H_0^*, R_0^*, c^* on t^* for a constant h^* and Ω. Evaluation of the disc's performance in various values of ω and Ω.

We highlighted the below interesting points, which have not been addressed in the study of Lin [8].

a) It has been considered to apply the idea of a stochastic process to the problem of SR in annular discs. In conjunction with abrasive bearing surfaces, two distinct models of hydrodynamic lubrication are created. The first of these models is associated with a 1-D, azimuthal roughness, and the second model applies to a 1-D radial roughness.

b) It has been proposed that disc coating has a two-part geometry. The large-scale portion of the film geometry, including any long wavelength disturbances, is measured in the first component, which will be referred to as the thickness of the nominal film. The second component of the film geometry is the part caused by SR, which is calculated from the nominal level and is thought to change at random.

c) By using Christensens stochastic theory, an averaged non-linear modified RE equation has been derived.

d) Probability density function, expectation, average, and variance are employed to reveal the impacts of c^* for P^*, W^* and t^*.

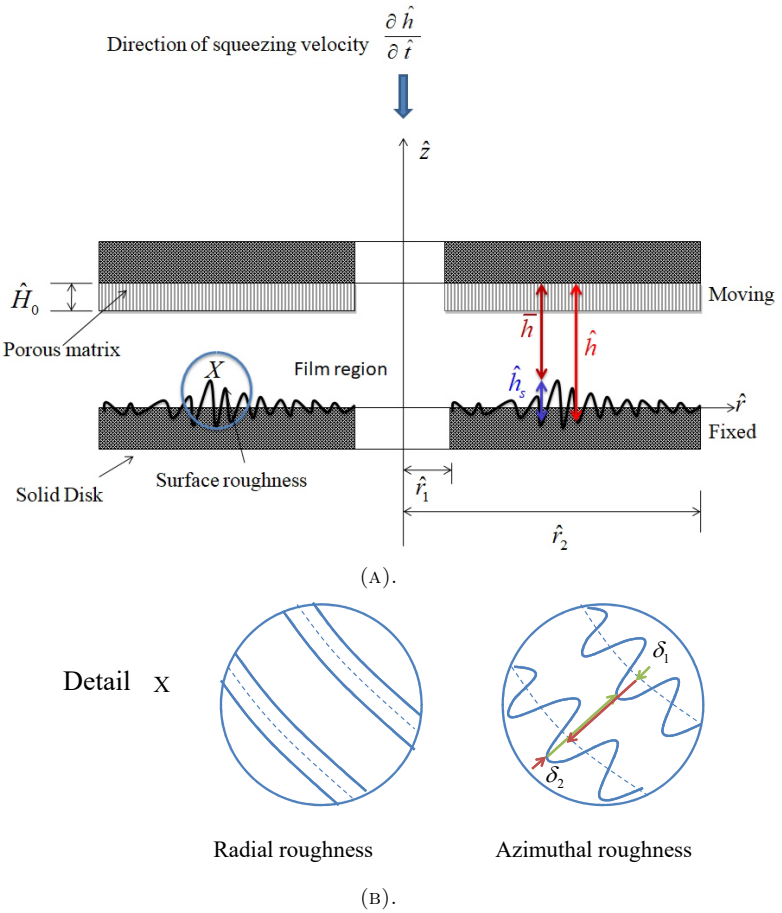

FIGURE 1. An illustrative picture showing the physical characteristics of a squeeze film design (A), with details of surface roughness of porous rough annular disks (B).

In the world of engineering and material science, the investigation of porous surfaces with particular roughness effects on annular discs is a fresh and fascinating topic of study. In annular discs, the combination of the notions of surface porosity and roughness is new and has significant implications for numerous applications. Here, we describe the novelty and possible objectives of this research work in this area.

1.2. NOVELTY

Exploring the interactions between surface porosity and roughness within annular discs is exclusive. Investigators can produce materials and structures with different characteristics and capacities by combining these two features, which is not possible by researching them separately. Incorporating porous and rough surfaces into circular discs can increase the effectiveness of heat transfer. Applications like heat exchangers, where an improved thermal performance can result in energy savings, are particularly interesting in this area. It is novel to understand how the interaction of porosity and roughness affects fluid flow within annular discs. The knowledge gained from this may be useful for fluidic devices, pumps, and turbines. To create specific porous and rough structures in annular discs for specialised purposes, such as biomedical devices, aircraft components, or filtration systems, novel surface modification techniques can be created.

1.3. OBJECTIVE

One of the primary objectives is to optimise the design of porous and rough annular discs for specific applications. Researchers can aim to maximise heat transfer efficiency, minimise pressure drop, or enhance filtration performance, depending on the application requirements. Simulations can be done by developing an analytical model to predict how different combinations of porosity and roughness affect fluid flow patterns and structural integrity within annular discs.

Overall, the objectives of the research in this area revolve around optimising the design, understanding the behaviour, and exploring the applications of annular discs with integrated porous and rough surfaces to meet the specific needs of various industries and technologies.

2. PROBLEM FORMULATION

The squeeze film, produced by two porous annular discs with inner and outer radii $\hat{r}_1$ and $\hat{r}_2$, moving toward one another at a squeeze velocity $(-\partial\hat{h}/\partial t)$, is shown in Figure 1. Porous media with thickness $\hat{H}_0$ and capillary radii $\hat{R}_0$ are present in the upper disc.

3. Mathematical formulations and solutions

The RFM is also known as the non-linear cubic power that correlates the shear stress $\tau_{\hat{r}\hat{z}}$ and strain rate $(\partial\hat{u}/\partial\hat{z})$. It is described mathematically as

$$\tau_{\hat{r}\hat{z}} = \hat{\mu}\frac{\partial\hat{u}}{\partial\hat{z}} - \varkappa\tau^3_{\hat{r}\hat{z}}, \tag{1}$$

where $\hat{\mu}$ is the dynamic viscosity of the NNF. The non-linear component $\varkappa$, which defines the feature of RFM, can be used to discriminate between three different types of fluids.

- The fluids are referred to as pseudo-plastic if $\varkappa > 0$,
- The fluids are referred to as Newtonian if $\varkappa = 0$,
- The fluids are referred to as dilatant if $\varkappa < 0$.

The following continuity and momentum equations have been used to govern the governing equations for the RFM (Lin [8]; Rahul et al. [14, 15]).

$$\frac{1}{\hat{r}}\frac{\partial(\hat{r}\hat{u})}{\partial\hat{r}} + \frac{\partial\hat{w}}{\partial z} = 0, \tag{2}$$

$$\frac{\partial p}{\partial\hat{r}} - \frac{\partial\tau_{\hat{r}\hat{z}}}{\partial\hat{z}} = 0, \tag{3}$$

$$\frac{\partial p}{\partial\hat{z}} = 0. \tag{4}$$

Rough porous annular disc boundary conditions are described by Equations 5 and 6.

a) At the upper surface:

$$\hat{z} = 0: \quad \hat{u}(\hat{r},0,\hat{t}) = 0, \quad \hat{w}(\hat{r},0,\hat{t}) = \hat{w}_{prs} \tag{5}$$

b) At the lower surface:

$$\hat{z} = \hat{h}: \quad \hat{u}(\hat{r},\hat{h},\hat{t}) = 0, \quad \hat{w}(\hat{r},\hat{h},\hat{t}) = -\frac{\partial\hat{h}}{\partial\hat{t}}, \tag{6}$$

where $\hat{u}(\hat{r},\hat{h},\hat{t})$ and $\hat{w}(\hat{r},\hat{h},\hat{t})$ are the components of velocity in $\hat{r}$ and $\hat{z}$ directions, respectively. $\hat{w}_{prs}$ is the velocity of a through-flow on the upper boundary of the porous layer.

The velocity component $\hat{u}$ is determined by substituting Equation 1 by the above Equation 3 and integrating while taking boundary conditions Equations 5 and 6 into consideration.

$$\hat{u}(\hat{r},\hat{z}) = \frac{1}{2\hat{\mu}}\left[G^{(0)}(\hat{h},\hat{z})\frac{\partial p}{\partial\hat{r}} + \varkappa\left(\frac{\partial p}{\partial\hat{r}}\right)^3 G^{(1)}(\hat{h},\hat{z})\right], \tag{7}$$

By substituting Equation 7 into Equation 2 and integrating with respect to $\hat{z}$, we obtained

$$\frac{1}{\hat{r}}\frac{\partial}{\partial\hat{r}}\left\{\hat{r}\int_{\hat{z}=0}^{\hat{z}=\hat{h}}\frac{1}{2\hat{\mu}}\left[G^{(0)}(\hat{h},\hat{z})\frac{\partial p}{\partial\hat{r}} + \varkappa\left(\frac{\partial p}{\partial\hat{r}}\right)^3 G^{(1)}(\hat{h},\hat{z})\right]d\hat{z}\right\} = -\int_{\hat{z}=0}^{\hat{z}=\hat{h}}\frac{\partial\hat{w}}{\partial\hat{z}}d\hat{z}. \tag{8}$$

The modified NLRE for the rough porous annular discs is given by applying the boundary conditions (5) and (6) into Equation 8 as follows:

$$\frac{1}{\hat{r}}\frac{\partial}{\partial\hat{r}}\left[\hat{r}\hat{h}^3\left\{\left(\frac{\partial p}{\partial\hat{r}}\right) + \frac{3}{20}\varkappa\hat{h}^2\left(\frac{\partial p}{\partial\hat{r}}\right)^3\right\}\right] = 12\mu\left[\frac{\partial\hat{h}}{\partial\hat{t}} - \hat{w}_{prs}\right]. \tag{9}$$

3.1. Porous wall

Let the non-Newtonian RF flow within the porous layer follow the modified Darcy's law and the layer be isotropic and homogeneously distributed. The capillary network that makes up these homogeneous, isotropic porous layers has an average radius of $\hat{R}_0$ and porosity $\hat{\psi}$. The axial and radial components of the velocity through the porous wall transform into

$$\hat{u}_p = \frac{\hat{\psi}}{\hat{\mu}}\left(-\frac{\partial\overline{p}}{\partial\hat{r}}\right) + \frac{\hat{\psi}}{\hat{\mu}}\frac{\varkappa\hat{R}_0^2}{6}\left(-\frac{\partial\overline{p}}{\partial\hat{r}}\right)^3, \tag{10}$$

$$\hat{w}_p = \frac{\hat{\psi}}{\hat{\mu}}\left(-\frac{\partial\overline{p}}{\partial\hat{z}}\right) + \frac{\hat{\psi}}{\hat{\mu}}\frac{\varkappa\hat{R}_0^2}{6}\left(-\frac{\partial\overline{p}}{\partial\hat{z}}\right)^3, \tag{11}$$

where $\hat{\phi}$ is the coefficient of porosity, $\hat{u}_p$, $\hat{w}_p$ and $\hat{\psi} = \hat{\phi}\hat{R}_0^2/8$ stand for the velocity components and permeability of porous layer, respectively. At the porous-fluids functionality, the cross-velocity component $\hat{w}_{prs}$ is always continuous and equals $\hat{w}_p$.

$$\text{i.e. } (\hat{w}_p)_{\text{at }\hat{z}=0} = (\hat{w}_{prs})_{\text{at }\hat{z}=0}. \tag{12}$$

Substituting Equation 12 into Equation 9, the result obtained is known as the modified NLRE which is expressed as:

$$\frac{1}{\hat{r}}\frac{\partial}{\partial\hat{r}}\left[\hat{r}\hat{h}^3\left\{\left(\frac{\partial p}{\partial\hat{r}}\right) + \frac{3}{20}\varkappa\hat{h}^2\left(\frac{\partial p}{\partial\hat{r}}\right)^3\right\}\right] = 12\hat{\mu}\left[\frac{d\hat{h}}{d\hat{t}} - \frac{\hat{\psi}}{\hat{\mu}}\left(-\frac{\partial\overline{p}}{\partial\hat{z}}\right) + \frac{\varkappa\hat{R}_0^2}{6}\left(-\frac{\partial\overline{p}}{\partial\hat{z}}\right)^3\right]_{\hat{z}=0}. \tag{13}$$

The modified version of Darcy's law satisfied Equation 2 for the porous layer (Walicka et al. [13], Rao and Rahul [14, 15])

$$\frac{1}{\hat{r}}\frac{\partial(\hat{r}\hat{u}_p)}{\partial\hat{r}} + \frac{\partial\hat{w}_p}{\partial\hat{z}} = 0. \tag{14}$$

By substituting Equation 10 and Equation 11 into Equation 14, we obtain

$$\frac{\partial}{\partial\hat{z}}\left[\left(-\frac{\partial\overline{p}}{\partial\hat{z}}\right) + \frac{\varkappa\hat{R}_0^2}{6}\left(-\frac{\partial\overline{p}}{\partial\hat{z}}\right)^3\right] = -\frac{1}{\hat{r}}\frac{\partial}{\partial\hat{r}}\left[\hat{r}\left\{\left(-\frac{\partial\overline{p}}{\partial\hat{r}}\right) + \frac{\varkappa\hat{R}_0^2}{6}\left(-\frac{\partial\overline{p}}{\partial\hat{r}}\right)^3\right\}\right], \tag{15}$$

Integrating Equation 15 with respect to $\hat{z}$ over the porous layer region $[-\hat{H}_0, 0]$,

$$\left[\left(-\frac{\partial\overline{p}}{\partial\hat{z}}\right)+\frac{\varkappa\hat{R}_0^2}{6}\left(-\frac{\partial\overline{p}}{\partial\hat{z}}\right)^3\right]_{\hat{z}=0} = -\frac{1}{\hat{r}}\frac{\partial}{\partial\hat{r}}\hat{r}\int\limits_{-\hat{H}_0}^{0}\left[\left(-\frac{\partial\overline{p}}{\partial\hat{r}}\right)+\frac{\varkappa\hat{R}_0^2}{6}\left(-\frac{\partial\overline{p}}{\partial\hat{r}}\right)^3\right]d\hat{z}, \tag{16}$$

since

$$\left[\left(-\frac{\partial\overline{p}}{\partial\hat{z}}\right)+\frac{\varkappa\hat{R}_0^2}{6}\left(-\frac{\partial\overline{p}}{\partial\hat{z}}\right)^3\right]_{\hat{z}=-\hat{H}_0} = 0, \tag{17}$$

For small $\hat{H}_0$, we obtain

$$\left[\left(-\frac{\partial\overline{p}}{\partial\hat{z}}\right)+\frac{\varkappa\hat{R}_0^2}{6}\left(-\frac{\partial\overline{p}}{\partial\hat{z}}\right)^3\right]_{\hat{z}=0} \approx \frac{-\hat{H}_0}{\hat{r}}\frac{\partial}{\partial\hat{r}}\left[\hat{r}\left\{\left(-\frac{\partial\overline{p}}{\partial\hat{r}}\right)+\frac{\varkappa\hat{R}_0^2}{6}\left(-\frac{\partial\overline{p}}{\partial\hat{r}}\right)^3\right\}\right]_{\hat{z}=0}. \tag{18}$$

Using the Morgan-Cameron approximation [11], the Equation 18 is used in Equation 13, the modified NLRE, which is defined as

$$\frac{1}{\hat{r}}\frac{\partial}{\partial\hat{r}}\left[\hat{r}\left\{f_1(\hat{h},\hat{\phi},\hat{R}_0,\hat{H}_0)\frac{\partial p}{\partial\hat{r}} + \frac{3}{20}\varkappa f_2(\hat{h},\hat{\phi},\hat{R}_0,\hat{H}_0)\left(\frac{\partial p}{\partial\hat{r}}\right)^3\right\}\right] = 12\hat{\mu}\left(\frac{d\hat{h}}{d\hat{t}}\right), \tag{19}$$

where

$$f_1(\hat{h},\hat{\phi},\hat{R}_0,\hat{H}_0) = \hat{h}^3 - \frac{3}{2}\hat{\phi}\hat{R}_0^2\hat{H}_0,$$
$$f_2(\hat{h},\hat{\phi},\hat{R}_0,\hat{H}_0) = \hat{h}^5 + \frac{5}{3}\hat{\phi}\hat{R}_0^4\hat{H}_0.$$

3.2. Surface roughness

In the case of surface roughness, the concept of film thickness is divided into two parts.

$$\hat{h} = \hat{h}(\hat{r}) + \hat{h}_s(\hat{r},\theta,\xi), \tag{20}$$

where $\hat{h}(\hat{r})$ represents the apparent smooth part of the film geometry, $\hat{h}_s = \delta_1 + \delta_2$ provides the arbitrary region resulting from SR irregularities measured from the apparent level, and ξ represents the irregular variable that represents the apparent positive definite roughness arrangement. The Gaussian distribution is used to calculate the roughness profile heights that are valid up to three standard deviations or more for a range of lubricated rough surfaces. A likelihood rough distribution function is defined by Christensen [16]:

$$f(\hat{h}_s) = \begin{cases}\frac{35}{32c^7}(c^2-\hat{h}_s^2)^3, & -c\le\hat{h}_s\le+c\\ 0, & \text{elsewhere}\end{cases} \tag{21}$$

where c denotes the maximum deviation from the mean film thickness, i.e., $c = \pm 3\sigma$, where σ is the standard deviation. Using expected values in Equation 21, we obtain the following equation of the averaged NLRE:

$$\frac{1}{\hat{r}}\frac{\partial}{\partial\hat{r}}\left[\hat{r}\left(E\left\{f_1(\hat{h},\hat{\phi},\hat{R}_0,\hat{H}_0)\right\}\frac{\partial E(p)}{\partial\hat{r}} + \frac{3}{20}\varkappa E\left\{f_2(\hat{h},\hat{\phi},\hat{R}_0,\hat{H}_0)\right\}\left(\frac{\partial E(p)}{\partial\hat{r}}\right)^3\right] = 12\hat{\mu}\frac{dE(\hat{h})}{d\hat{t}}. \tag{22}$$

The expectation operator $E(\cdot)$ is expressed as follows:

$$E(\cdot) = \int\limits_{-c}^{+c}(\cdot)f(h_s)dh_s. \tag{23}$$

By using stochastic theory, Christensen [16] has proposed two different types of 1-D roughness patterns: azimuthal and radial patterns. The patterns of roughness are confined edges and valleys flowing in the same direction. The film thickness region for the one-dimensional radial and azimuthal roughness is represented as follows:

$$\hat{h} = \begin{cases}\hat{h}(\hat{r}) + \hat{h}_s(\theta,\xi), & \text{radial roughness}\\ \hat{h}(\hat{r}) + \hat{h}_s(\hat{r},\xi), & \text{azimuthal roughness.}\end{cases} \tag{24}$$

For these roughness patterns, the modified stochastic NLRE is given by

$$\frac{1}{\hat{r}}\frac{\partial}{\partial\hat{r}}\left[\hat{r}\left\{G_1(\hat{h},\hat{\phi},\hat{R}_0,\hat{H}_0)\frac{\partial E(p)}{\partial\hat{r}} + \frac{3}{20}\varkappa G_2(\hat{h},\hat{\phi},\hat{R}_0,\hat{H}_0)\left(\frac{\partial E(p)}{\partial\hat{r}}\right)^3\right\}\right] = 12\hat{\mu}\frac{dE(\hat{h})}{d\hat{t}}. \tag{25}$$

where

$$G_1(\hat{h},\hat{\phi},\hat{R}_0,\hat{H}_0,c) = \begin{cases}E\{f_1(\hat{h},\hat{\phi},\hat{R}_0,\hat{H}_0)\}, & \text{radial roughness}\\ \left[E\left\{1/f_1(\hat{h},\hat{\phi},\hat{R}_0,\hat{H}_0)\right\}\right]^{-1}, & \text{azimuthal roughness.}\end{cases} \tag{26}$$

$$G_2(\hat{h},\hat{\phi},\hat{R}_0,\hat{H}_0,c) = \begin{cases}E\{f_2(\hat{h},\hat{\phi},\hat{R}_0,\hat{H}_0)\}, & \text{radial roughness}\\ \left[E\left\{1/f_2(\hat{h},\hat{\phi},\hat{R}_0,\hat{H}_0)\right\}\right]^{-1}, & \text{azimuthal roughness.}\end{cases}$$

Currently, the problem is minimising the constructing methods for estimating the left side of Equation 25 according to a specified roughness pattern. The measurement of mean FP involves the evaluation of the standard estimate of distinct film thicknesses. The probability density function is incorporated by Equation 21. The accompanying expected estimations of film thickness is discussed in the work by Walicka et al. [23].

$$
\begin{aligned}
E(\hat{h}) &= \hat{h},\\
E(\hat{h}^2) &= \hat{h}^2\left(1+\frac{\Delta^2}{9}\right),\\
E(\hat{h}^3) &= \hat{h}^3\left(1+\frac{\Delta^2}{3}\right),\\
E(\hat{h}^4) &= \hat{h}^4\left(1+\frac{2\Delta^2}{3}+\frac{\Delta^4}{33}\right),\\
E(\hat{h}^5) &= 5\hat{h}^5\left(1+\frac{2\Delta^2}{5}+\frac{\Delta^4}{33}\right),\\
E(\hat{h}^6) &= 5\hat{h}^6\left(\frac{1}{5}+\frac{\Delta^2}{93}+\frac{\Delta^4}{11}+\frac{\Delta^6}{429}\right),\\
E(\hat{h}^{-1}) &= \frac{1}{\hat{h}}\left[\frac{35}{32}\frac{1}{\Delta^7}\left\{(\Delta^2-1)\ln\left(\frac{1+\Delta}{1-\Delta}\right)\right.\right.\\
&\quad\left.\left.-\frac{2\Delta}{15}\left(15-40\Delta^2+33\Delta^4\right)\right\}\right],\\
E(\hat{h}^{-2}) &= \frac{1}{\hat{h}^2}\left[\frac{35}{32}\frac{1}{\Delta^7}\left\{6(\Delta^2-1)\ln\left(\frac{1+\Delta}{1-\Delta}\right)\right.\right.\\
&\quad\left.\left.-\frac{4\Delta}{5}\left(15-25\Delta^2+8\Delta^4\right)\right\}\right],\\
E(\hat{h}^{-3}) &= \frac{1}{\hat{h}^3}\left[\frac{35}{32}\frac{1}{\Delta^7}\left\{3(5-\Delta^2)(\Delta^2-1)\ln\left(\frac{1+\Delta}{1-\Delta}\right)\right.\right.\\
&\quad\left.\left.+2\Delta\left(15-13\Delta^2\right)\right\}\right],\\
E(\hat{h}^{-4}) &= \frac{1}{\hat{h}^4}\left[\frac{35}{32}\frac{1}{\Delta^7}\left\{4(5-3\Delta^2)\ln\left(\frac{1+\Delta}{1-\Delta}\right)\right.\right.\\
&\quad\left.\left.-\frac{8\Delta}{3}\left(15-4\Delta^2\right)\right\}\right],\\
E(\hat{h}^{-5}) &= \frac{1}{\hat{h}^5}\left[\frac{35}{32}\frac{1}{\Delta^7}\left\{3(\Delta^2-5)\ln\left(\frac{1+\Delta}{1-\Delta}\right)\right.\right.\\
&\quad\left.\left.+\frac{2\Delta}{1+\Delta^2}\left(15-13\Delta^2\right)\right\}\right],\\
E(\hat{h}^{-6}) &= \frac{1}{\hat{h}^6}\left[\frac{35}{32}\frac{1}{\Delta^7}\left\{3\ln\left(\frac{1+\Delta}{1-\Delta}\right)\right.\right.\\
&\quad\left.\left.+\frac{2\Delta}{5(1-\Delta^2)}\left(15-25\Delta^2+8\Delta^4\right)\right\}\right].
\end{aligned}
\tag{27}
$$

where

$$\Delta = \frac{c}{\hat{h}}. \tag{28}$$

The predicted values of film thickness feature $E\left(\hat{h}^{-i}\right)$, $i = 1, 2, \ldots, 6$, are not suitable for numerical purposes for small Δ values, as there are variations when small amounts are involved, resulting in a loss in large digits. Hence, expansions of Taylors powers Δ are proposed. The expansion of these film thickness functions in series

$$
\begin{aligned}
E(\hat{h}^{-1}) &= \frac{1}{\hat{h}}\left[1+\sum_{n=1}^{\infty}\frac{105\Delta^{2n}}{(2n+1)(2n+3)(2n+5)(2n+7)}\right],\\
E(\hat{h}^{-2}) &= \frac{1}{\hat{h}^2}\left[1+\sum_{n=1}^{\infty}\frac{105\Delta^{2n}}{(2n+3)(2n+5)(2n+7)}\right],\\
E(\hat{h}^{-3}) &= \frac{1}{\hat{h}^3}\left[1+\sum_{n=1}^{\infty}\frac{105(n+1)\Delta^{2n}}{(2n+3)(2n+5)(2n+7)}\right],\\
E(\hat{h}^{-4}) &= \frac{1}{\hat{h}^4}\left[1+\sum_{n=1}^{\infty}\frac{35(n+1)\Delta^{2n}}{(2n+5)(2n+7)}\right],\\
E(\hat{h}^{-5}) &= \frac{1}{\hat{h}^5}\left[1+\sum_{n=1}^{\infty}\frac{35(n+1)(n+2)\Delta^{2n}}{2(2n+5)(2n+7)}\right],\\
E(\hat{h}^{-6}) &= \frac{1}{\hat{h}^6}\left[1+\sum_{n=1}^{\infty}\frac{7(n+1)(n+2)\Delta^{2n}}{2(2n+7)}\right].
\end{aligned}
\tag{29}
$$

The pressure boundary conditions for the NLRE are given by Equation 30

$$
\begin{cases}
\hat{p}=0 \quad \text{at} \quad \hat{r}=\dfrac{\hat{r}_1}{\hat{r}_2},\\
\hat{p}=0 \quad \text{at} \quad \hat{r}=1.
\end{cases}
\tag{30}
$$

Introducing the dimensionless variables and parameters:

$$
\begin{gathered}
r^* = \frac{\hat{r}}{\hat{r}_2}, \quad h^* = \frac{\hat{h}}{\hat{h_0}}, \quad H^* = \frac{\hat{H}}{\hat{h_0}}, \quad R^* = \frac{\hat{R}}{\hat{h_0}},\\
\Omega = \frac{\hat{r}_1}{\hat{r}_2}, \quad c^* = \frac{c}{\hat{h_0}},\\
P^* = \frac{p\hat{h_0}^3}{\hat{\mu}_0\hat{r}_2^2(-d\hat{h}/d\hat{t})}, \quad \omega = \frac{\varkappa\hat{\mu}_0^2\hat{r}_2^2(-d\hat{h}/d\hat{t})}{\hat{h}_0^4}.
\end{gathered}
\tag{31}
$$

Under the above mentioned dimensionless variables and parameters, the NLRE Equation 25 is expressed as:

$$
\begin{aligned}
&\frac{\partial}{\partial r^*}\left[r^*G_1^*(h^*,R_0^*,H_0^*,c^*)\left(\frac{\partial P^*}{\partial r^*}\right)\right.\\
&\left.+\frac{3}{20}\omega G_2^*(h^*,R_0^*,H_0^*,c^*)\left(\frac{\partial P^*}{\partial r^*}\right)^3\right] = -12r^*,
\end{aligned}
\tag{32}
$$

where

$$
\begin{gathered}
G_1(h^*,R^*,H^*,c^*) =\\
\begin{cases}
E\{f_1(h^*,R_0^*,H_0^*)\}, & \text{radial roughness}\\
\left[E\left\{1/f_1^*(h^*,R_0^*,H_0^*)\right\}\right]^{-1}, & \text{azimuthal roughness}
\end{cases}
\end{gathered}
\tag{33}
$$

$$G_2(h^*, R^*, H^*, c^*) = \begin{cases} E\{f_2(h^*, R_0^*, H_0^*)\}, & \text{radial roughness} \\ [E\{1/f_2^*(h^*, R_0^*, H_0^*)\}]^{-1}, & \text{azimuthal roughness} \end{cases} \quad (34)$$

where ω represents the non-dimensional non-linear factor that specifies the RF behaviour. If, $\omega = 0$ the fluids will behave like NF; $\omega > 0$, the fluids will decompose as pseudoplastic fluids and $\omega < 0$, the fluids will be dilatant fluids.

The boundary condition in terms of dimensionless form is:

$$\left.\begin{aligned} P^* = 0 \quad \text{at} \quad r^* = \Omega, \\ P^* = 0 \quad \text{at} \quad r^* = 1. \end{aligned}\right\} \quad (35)$$

The value of the pseudoplastic coefficient $\varkappa$ depends on the type and quantity of additives which can be determined experimentally [7]. Thus, the values of ω can be calculated with the appropriate value of $\varkappa$. However, for the validity of the present analysis, the value of ω is restricted to $|\omega| < 0.01$. It is discovered that the dimensionless non-Newtonian averaged modified NLRE is nonlinear in terms of P^*. A small perturbation method based on Lin [8], Rahul and Rao [14, 15, 24] is used to get approximate analytical solutions.

Therefore, the classical perturbation method is used to solve it. The perturbation series for P can be expressed in the form:

$$P^* = P_0^* + \omega P_1^* + \omega^2 P_2^* + \ldots \quad (36)$$

For $\omega \ll 1$, it is sufficient, for the analysis, to consider the first order term in ω as follows: For small values of the nonlinear parameter ω, the FP is perturbed:

$$P^* = P_0^* + \omega P_1^*, \quad (37)$$

For the higher values of ω, second and higher-order terms can be considered to increase the accuracy of the results. However, for the higher values of ω, it is more appropriate to adopt a numerical solution procedure such as the finite element method to solve the Reynolds equation.

To obtain the FP P_0^* and P_1^*, we substitute Equation 37 into the modified NLRE Equation 32

$$\frac{\partial}{\partial r^*}\left[r^* G_1^*(h^*, R_0^*, H_0^*, c^*)\left(\frac{\partial P^*}{\partial r^*}\right)\right] + 12r^* = 0, \quad (38)$$

$$\frac{\partial}{\partial r^*}\left[r^* G_1^*(h^*, R_0^*, H_0^*, c^*)\left(\frac{\partial P^*}{\partial r^*}\right)\right] = -\frac{3}{20} G_2^*(h^*, R_0^*, H_0^*, c^*)\frac{\partial}{\partial r^*}\left[r\left(\frac{\partial P_0^*}{\partial r^*}\right)^3\right]. \quad (39)$$

After solving Equation 38 and Equation 39, the perturbed dimensionless film pressures P_0^* and P_1^* are:

$$P_0^* = \frac{3}{G_1^*(h^*, R_0^*, H_0^*, c^*)}\left[1 - r^{*2} + \left(\frac{\Omega^2 - 1}{\log \Omega}\right)\log r^*\right], \quad (40)$$

$$P_1^* = -\frac{A_4}{G_1^*(h^*, R_0^*, H_0^*, c^*)}\log r^* - \frac{3}{20}\frac{G_2^*(h^*, R_0^*, H_0^*, c^*)}{G_1^*(h^*, R_0^*, H_0^*, c^*)} \left\{\left[54(1 - r^{*4}) - 54A_4(1 - r^{*2}) - 18A_4^2 \log r^*\right] + \frac{1}{2}A_4^3\left(\frac{1}{r^{*2}} - 1\right)\right\}, \quad (41)$$

where

$$A_4 = -\frac{3(1 - \Omega^2)}{\log \Omega}$$

$$A_2 = \frac{3}{20}\frac{G_2^*(h^*, R_0^*, H_0^*, c^*)}{G_1^{*4}(h^*, R_0^*, H_0^*, c^*)} \frac{1}{\log \Omega}\left\{54(1 - r^{*4}) - 54A_4(1 - \Omega^2) - 18A_4^2 \log S + \frac{1}{2}A_4^3\left(\frac{1}{\Omega^2} - 1\right)\right\}. \quad (42)$$

The FP is integrated into the domain $[\hat{r}_1, \hat{r}_2]$ to get the LCC of annular discs.

$$W = 2\pi \int_{\hat{r}_1}^{\hat{r}_2} p\hat{r}d\hat{r}. \quad (43)$$

The dimensionless form of Equation 43 is given below:

$$W^* = \frac{\hat{W}\hat{h}_0^3}{\hat{\mu}_0 \hat{r}_2^4(-d\hat{h}/dt)} = 2\pi \int_{\Omega}^{1} P^* r^* dr^*. \quad (44)$$

Introducing the dimensionless SRT as:

$$t^* = \frac{W\hat{h}_0^2}{\hat{\mu}_0 \hat{r}_2^4}\hat{t}, \quad (45)$$

Substituting Equation 45 into Equation 44 yields the ordinary differential equation that incorporates the film height, which varies with SRT.

$$\frac{dh^*}{dt^*} = -\frac{1}{W^*}. \quad (46)$$

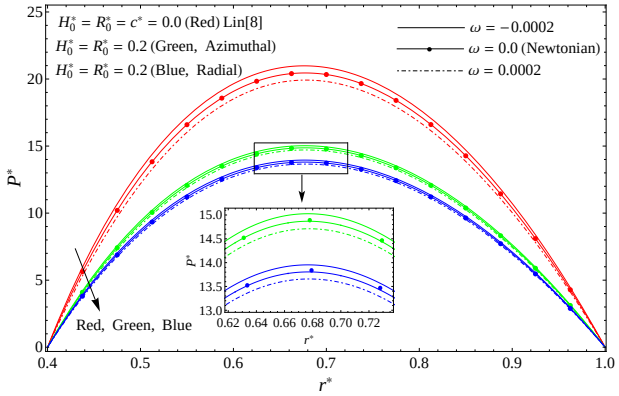

Figure 2. Variations in FP (P^*) with a coordinate axis (r^*) for different values of ω, H_0^* and R_0^* with $\Omega = 0.4$ and $c^* = 0.1$ and $h^* = 0.3$.

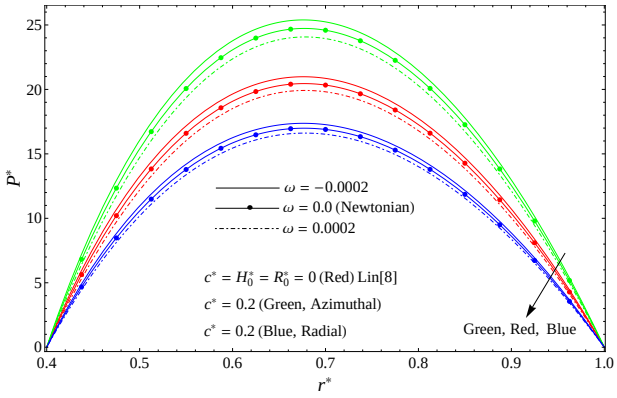

Figure 3. Variations in FP (P^*) with a coordinate axis (r^*) for different values of ω and c^* with $\Omega = 0.4$, $h^* = 0.3$ and $H_0^* = 0.1$ and $R_0^* = 0.1$.

The non-dimensional film thickness $t^* = 0$ is initially under the condition of $h^* = 1$. Integrate this equation while using the initial condition:

$$t^* = \int_{h^*}^{1} \frac{1}{W^*} dh^*. \tag{47}$$

With the use of the Gaussian quadrature integration algorithm, we were able to determine the properties of the discs by applying the boundary conditions and including the variable.

4. Results and Discussion

The characteristics of a squeeze film between porous rough annular discs under RFM are investigated and the results of this study are represented in the form of graphs and tables. In the beginning of this study, Darcy's law and Morgan-Cameron approximation are chosen for NNF in the porous matrix condition with homogeneous capillary tubes and the Christensen stochastic theory for surface roughness (SR) on annular discs. For this given special case, the value of $\omega \to 0$.

$$\frac{\partial}{\partial r^*}\left[r^*\left\{G_1^*(h^*, R_0^*, H_0^*, c^*)\left(\frac{\partial P^*}{\partial r^*}\right)\right\}\right] = -12r^*. \tag{48}$$

As the porous, roughness, and viscosity variation parameters tend to zero ($H_0^* \to 0$, $R_0^* \to 0$, $c^* \to 0$), the results are obtained, as was also in the case of Lin [8]. Also, one can obtain the corresponding cases from the specific values of the parameters.

- $H_0^* = R_0^* = 0$: the non-porous case;
- $c^* = 0$: smooth surface;
- $\omega = 0$: the NF case; and

Some representative values being used for RF, porosity, and SR can be observed in many articles such as Lin [8], Walicka et al. [32], and Siddangouda et al. [9].

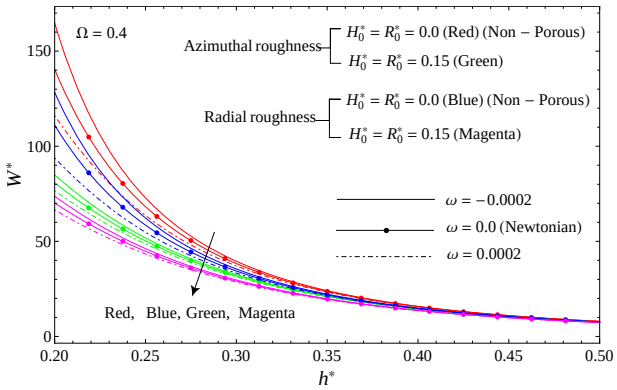

Figure 4. Variations in LCC (W^*) with h^* for different values of ω, H_0^* and R_0^* with $c^* = 0.1$ and $\Omega = 0.4$.

In addition, the following set of parameters is used when performing numerical calculations: RF nonlinear parameter: $\omega \in [-0.0002, 0.0002]$, roughness parameter: $c^* = 0, 0.1, 0.2, 0.3, 0.4$ relative porous parameter: $H_0^* = 0.0, 0.1, 0.2$ and $R^* = 0.0, 0.1, 0.2$.

In this section, the solid lines demonstrate the dilatant fluids, dot-dashed lines represent the pseudoplastic fluids, and the solid lines with a solid circle marker represent the Newtonian fluids. Figure 2 describes how the FP distribution over the porous hydrodynamic annular discs varies along with different r^* values of the porous and RF parameters under fixed $\Omega = 0.4$, $h^* = 0.3$ and $c^* = 0.1$. It is observed that FP decreases with respect to increasing porosity, which is a similar trend to that observed by Lin [8]. In addition, the effect of RF on porous wall increases the FP for dilatant fluids whereas pseudoplastic fluids behaviour shows a reverse trend as compared to NF. Figure 3 shows the effect of squeeze FP (P^*) along with the coordinate axis (r^*) for different values of ω and c^* with $\Omega = 0.4$, $h^* = 0.3$, $H_0^* = 0.1$ and $R^* = 0.1$. It is shown that FP decreases with c^* for both types of roughness and finds a similar trend for RF with the smooth surface case of Lin [8].

Figures 4 and 5 illustrate the variation of LCC

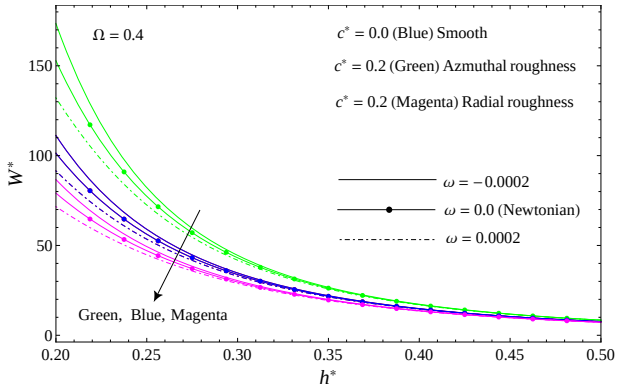

FIGURE 5. Variations in LCC (W^*) with h^* for different values of ω and c^* with $H_0^* = R_0^* = 0.1$ and $\Omega = 0.4$.

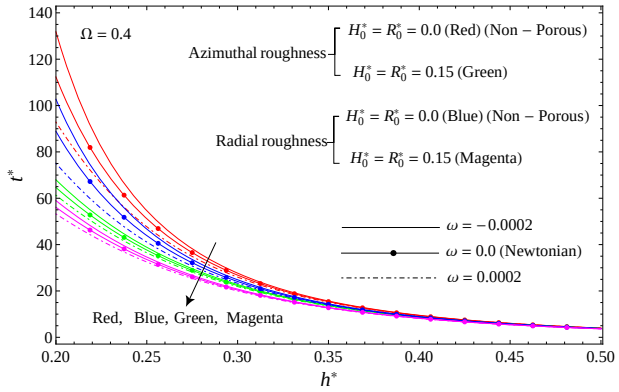

FIGURE 6. Variations in SRT (t^*) with h^* for different values of ω, H_0^* R_0^* with $c^* = 0.1$ and $\Omega = 0.4$.

(W^*) as a function of film thickness (h^*), influenced by the presence of porosity (H_0^* and R_0^*) and surface roughness (c^*) between annular discs. These variations are observed using the Rabinowitsch fluid model parameter (ω), while maintaining a constant radius ratio $\Omega = 0.4$. From these Figures 4 and 5, it is concluded that the effect of roughness plays a vital role in the LCC of the annular discs. Compared to the cases of the non-porous and smooth surface of discs, it is concluded that the impact of porosity and roughness reduces the LCC with increased film thickness. LCC also considerably decreases with the increasing porous parameter. Mostly in the case of roughness patterns, LCC is much more prominent as compared to a smooth surface for the azimuthal roughness. For lower and higher values of radius ratio, moreover, the effect of the dilatant fluids provides a larger LCC influence on the pseudoplastic fluids and is expected to yield inverse outcomes as compared to NF. Figures 6 demonstrates the the disparity of dimensionless SRT (t^*) concerning dimensionless film thickness (h^*) for distinct values of the non-linear parameter (ω), porous parameters (H_0^*, and R_0^*) under the radius ratio $\Omega = 0.4$. The impact of the porous media on discs, SRT is hugely prominent for the non-porous ($H_0^* = 0.0$, $R_0^* = 0.0$) as compared to the porous

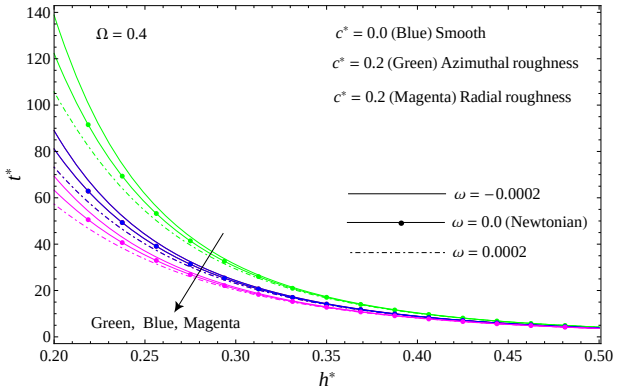

FIGURE 7. Variations in SRT (t^*) with h^* for different values of ω, and c^* with $H_0^* = R_0^* = 0.1$ and $\Omega = 0.4$.

case of discs. Influence of RF in the porous medium between annular discs, the SRT is lower for pseudoplastic and higher for dilatant fluids as compared to NF. Figures 7 shows the behaviour of SRT t^* against h^* with ω and c^* under the radius ratio $\Omega = 0.4$. It is found that t^* increases (decreases) for the azimuthal (Radial) roughness patterns. The SR accounted for more SRT with the lower radius ratio with respect to higher values of the radius ratio.

Tables 1 and 2 illustrate the numerical comparison of LCC with the results of Lin [8] (with $H_0^* = R_0^* = 0.0$, $h^* = 0.2$) and the present analysis for different values of ω, c^* and Ω. It can be concluded that increasing the roughness and porous parameters leads to a decrease in LCC. Moreover, dilatant fluids (-0.0002) showed a higher LCC as compared to pseudoplastic fluids ($+0.0002$).

5. CONCLUSIONS

Based on the RFM, the performance of annular discs under the condition of SR and the porous wall is studied in the present work proposing two different theories.

- The modified Darcy's law and Morgan-Cameron approximation for porous wall;
- Christensen's stochastic theory for SR.

The non-linear Reynolds equation (NLRE) is constructed using the above theories. To solve the NLRE, we used the techniques listed below:

- Small perturbation techniques;
- Five-point Gauss quadrature integral formula.

The annular discs are studied in two physical situations with surfaces: one with porous walls of equal thickness and radius of the capillarity tube, another with SR. FP, LCC, and SRT are calculated for different parameters of porous and SR. In the case of non-porous and smooth surfaces, the FP distribution, LCC, and SF are identical to the literature Lin [8]. The conclusions are as follows:

ω	$\Omega = 0.2$				$\Omega = 0.4$			
	Lin [8]		Present analysis		Lin [8]		Present analysis	
	$c^* = 0.0$ (Radial)	$c^* = 0.0$ (Azimuthal)	$c^* = 0.4$ (Radial)	$c^* = 0.4$ (Azimuthal)	$c^* = 0.0$ (Radial)	$c^* = 0.0$ (Azimuthal)	$c^* = 0.4$ (Radial)	$c^* = 0.4$ (Azimuthal)
−0.0002	329.088	329.088	69.7214	459.684	138.991	138.991	32.6894	197.561
0	250.804	250.804	66.5346	364.434	120.365	120.365	31.9312	174.899
+0.0002	172.519	172.519	63.3478	269.185	101.74	101.74	31.173	152.237

Table 1. Numerical comparison of LCC (W^*) of Lin [8] (with $H_0^* = R_0^* = 0.0$, $h^* = 0.2$) and present analysis (with $H_0^* = R_0^* = 0.1$, $h^* = 0.2$) for different values of ω, c^* and Ω.

ω	$\Omega = 0.2$ Lin[8]		Present analysis $H_0^* = R_0^* = 0.2$		$\Omega = 0.4$ Lin[8]		Present analysis $H_0^* = R_0^* = 0.2$	
	$H_0^* = 0.0$ $R_0^* = 0.0$ (Radial)	$H_0^* = 0.0$ $R_0^* = 0.0$ (Azimuthal)	$H_0^* = 0.2$ $R_0^* = 0.2$ (Radial)	$H_0^* = 0.2$ $R_0^* = 0.2$ (Azimuthal)	$H_0^* = 0.0$ $R_0^* = 0.0$ (Radial)	$H_0^* = 0.0$ $R_0^* = 0.0$ (Azimuthal)	$H_0^* = 0.2$ $R_0^* = 0.2$ (Radial)	$H_0^* = 0.2$ $R_0^* = 0.2$ (Azimuthal)
−0.0002	329.088	329.088	66.4727	72.9544	138.991	138.991	31.5269	34.5767
0	250.804	250.804	64.9249	71.155	120.365	120.365	31.1587	34.1486
+0.0002	172.519	172.519	63.377	69.3557	101.74	101.74	30.7904	33.7205

Table 2. Numerical comparison of LCC (W^*) of Lin [8] (with $h^* = 0.2$, $c^* = 0.0$) and present analysis (with $h^* = 0.2$, $c^* = 0.1$) for different values of ω, H_0^*, R_0^*, and Ω.

a) Annular discs with the presence of a porous wall: The FP, LCC, and SRT decrease as compared to non-porous discs, as in the case of Lin [8].

b) Annular discs with the presence of SR: The FP, LCC, and SRT decrease as compared with smooth discs, as in the case of Lin [8]. All these characteristics show a lower value for radial surface roughness (SR).

c) Annular discs with RFM: The performance of annular discs is better for dilatant fluids and lower for pseudoplastic fluids as compared to NF.

d) A radial roughness pattern on the porous surface of an annular disc can promote better fluid mixing and increase heat transfer efficiency. Radial roughness, on the other hand, can cause higher pressure drop and increased flow resistance, which can be a disadvantage in certain applications where energy efficiency and low-pressure losses are critical.

e) An annular disc's circumferential azimuthal roughness pattern can influence the flow of fluid in one direction, the amount of turbulence present inside the disc, and the flow velocity in various annular disc sections.

6. Future research

In conclusion, the study of porous roughness annular discs is an important are of research with several applications in fluid dynamics, materials science, and engineering. Several promising directions stand out as having high potential for future research in this area, including advanced materials and fabrication techniques, optimisation of porous structure, numerical modelling, and simulation, applications in energy and environmental engineering, surface modification techniques, data-driven approaches, etc. We can learn much more about porous roughness annular discs and unlock their potential to solve challenging problems across a range of industries by incorporating these research directions. Researchers can help make future engineering solutions more effective and sustainable by improving their design, performance, and applications.

List of symbols

Acronyms

FP Film pressure
NF Newtonian fluids
NLRE Non-linear Reynolds equation
NNF Non-Newtonian fluids
RFM Rabinowitsch fluid model
SF Squeeze film
SR Surface roughness
SRT Squeeze response time

Symbols

$\hat{r}_1, \hat{r}_2$ The outer/inner radius of annular discs [m]
Ω The ratio of inner and outer radius, $\Omega = \hat{r}_1/\hat{r}_2$ [–]
$\hat{h}_0, \hat{h}_1$ Inlet/outlet film thickness [m]
$\overline{h}$ Nominal film height [m]
$\hat{h}, h^*$ Film thickness ($\hat{h} = \overline{h} + \overline{h}_s$), $h^* = \hat{h}/\hat{h}_0$ [m]
$\overline{h}_s$ Film height deviation from the nominal level [m]
$E(\cdot)$ Expected value [–]
c, c^* The greatest asperity variation from the nominal height, $c^* = c/\hat{h}_0$ [–]
$d\hat{h}/d\hat{t}$ Squeeze velocity [$\mathrm{m\,s^{-1}}$]

$\hat{r}, \hat{z}, r^*$ Coordinates of discs, $r^* = \hat{r}/\hat{r}_2$ [–]

$\hat{w}_{prs}$ Through-flow velocity on the upper boundary of the porous layer [$\mathrm{m\,s^{-1}}$]

$\hat{u}, \hat{w}$ Velocity components in $\hat{r}$ and $\hat{z}$ directions [$\mathrm{m\,s^{-1}}$]

$\hat{u}_p, \hat{w}_p$ Axial and radial velocity component of the porous region. [$\mathrm{m\,s^{-1}}$]

$\hat{H}_0, H_0^*$ Porous pad thickness, $H_0^* = \hat{\phi}\hat{H}_0/\hat{h}_0$ [m]

$\hat{R}_0, R_0^*$ Porous pad thickness, $H_0^* = \hat{\phi}\hat{R}_0/\hat{h}_0$ [m]

$\overline{p}$ Film pressure in the porous region [Pa]

p, P^* Squeeze film pressure, $P^* = p\hat{h}_0^3/\hat{\mu}_0\hat{r}_2^2(-\partial\hat{h}/\partial\hat{t})$ [Pa]

W, W^* Load-carrying capacity, $W^* = W\hat{h}_0^3/\hat{\mu}_0\hat{r}_2^4(-\partial\hat{h}/\partial\hat{t})$ [N]

W, W^* Squeeze response time, $t^* = W\hat{h}_0^2\hat{t}/\hat{\mu}_0\hat{r}_2^4$ [s]

$\hat{\mu}$ Dynamic viscosity of the NNF [Po]

$\tau_{\hat{r}\hat{z}}$ Element of the stress tensor [Pa]

$\hat{\psi}$ Permeability of the porous region [$\mathrm{m^2}$]

$\hat{\mu}$ Coefficient of porosity [pu]

$\hat{\phi}$ Dynamic viscosity of the NNF [Po]

$\varkappa$ Nonlinear factor accounting for the Rabinowitsch fluid model [–]

ω Dimensionless non-linear factor, $\omega = \varkappa\hat{\mu}_0^2\hat{r}_2^2(-\partial\hat{h}/\partial\hat{t})/\hat{h}_0^4$ [–]

θ Circumferential co-ordinate [°]

ξ Random variable for surface roughness [–]

References

[1] C. Allen, A. McKillop. An investigation of the squeeze film between rotating annuli. *ASME Journal of Lubrication Technology* **92**(3):435–441, 1970. https://doi.org/10.1115/1.3451435

[2] N. Naduvinamani, A. Siddangouda, A. Kadadi, S. Biradar. Effect of pressure dependent viscosity on squeeze film characteristics of micropolar fluid in convex curved plates. *Tribology-Materials, Surfaces & Interfaces* **9**(3):154–158, 2015. https://doi.org/10.1080/17515831.2015.1107239

[3] H. Spikes. The behaviour of lubricants in contacts: current understanding and future possibilities. *Proceedings of the Institution of Mechanical Engineers, Part J: Journal of Engineering Tribology* **208**(1):3–15, 1994. https://doi.org/10.1243/PIME_PROC_1994_208_345_02

[4] J. Lin, C. Hung. Combined effects of non-Newtonian rheology and rotational inertia on the squeeze film characteristics of parallel circular discs. *Proceedings of the Institution of Mechanical Engineers, Part J: Journal of Engineering Tribology* **222**(4):629–636, 2008. https://doi.org/10.1243/13506501JET39

[5] Y. Wang, J. H. Wu, L. Xu. Influence of power-law fluid on transient performance of liquid film seal based on the time-dependent non-Newtonian dynamic reynolds equation. *Tribology International* **159**:106984, 2021. https://doi.org/10.1016/j.triboint.2021.106984

[6] S. Wada, H. Hayashi. Hydrodynamic lubrication of journal bearings by pseudo-plastic lubricants: part 1, theoretical studies. *Bulletin of JSME* **14**(69):268–278, 1971. https://doi.org/10.1299/jsme1958.14.268

[7] S. Wada, H. Hayashi. Hydrodynamic lubrication of journal bearings by pseudo-plastic lubricants: part 2, experimental studies. *Bulletin of JSME* **14**(69):279–286, 1971. https://doi.org/10.1299/jsme1958.14.279

[8] J.-R. Lin. non-Newtonian squeeze film characteristics between parallel annular disks: Rabinowitsch fluid model. *Tribology international* **52**:190–194, 2012. https://doi.org/10.1016/j.triboint.2012.02.017

[9] A. Siddangouda, N. Naduvinamani, S. Siddapur. Effect of surface roughness on the static characteristics of inclined plane slider bearing: Rabinowitsch fluid model. *Tribology-Materials, Surfaces & Interfaces* **11**(3):125–135, 2017. https://doi.org/10.1080/17515831.2017.1347745

[10] N. Bujurke, M. Jagadeeswar, P. Hiremath. Analysis of normal stress effects in a squeeze film porous bearing. *Wear* **116**(2):237–248, 1987. https://doi.org/10.1016/0043-1648(87)90236-5

[11] V. Morgan, A. Cameron. Mechanism of lubrication in porous metal bearings. In *International Proceeding Conference Lubrication and Wear, Institute of Mechanical Engineering*, vol. 89, pp. 151–157. Inst. Mech. Eng London, 1957.

[12] N. C. Patel, J. R. Patel, G. M. Deheri. A comparative study of ferrofluid lubrication on double-layer porous squeeze curved annular plates with slip velocity. *Acta Polytechnica* **62**(4):488–497, 2022. https://doi.org/10.14311/AP.2022.62.0488

[13] M. Bhat, G. Deberi. Squeeze film behaviour in porous annular discs lubricated with magnetic fluid. *Wear* **151**(1):123–128, 1991. https://doi.org/10.1016/0043-1648(91)90352-U

[14] A. Walicka, E. Walicki, P. Jurczak, J. Falicki. Curvilinear squeeze film bearing with rough surfaces lubricated by a Rabinowitsch–Rotem–Shinnar fluid. *Applied Mathematical Modelling* **40**(17-18):7916–7927, 2016. https://doi.org/10.1016/j.apm.2016.03.048

[15] P. Rao, A. Rahul, S. Agarwal. Effect of non-Newtonian lubrication of squeeze film conical bearing with the porous wall operating with Rabinowitsch fluid model. *Proceedings of the Institution of Mechanical Engineers, Part J: Journal of Engineering Tribology* **232**(10):1293–1303, 2018. https://doi.org/10.1177/1350650117749735

[16] P. Rao, A. Rahul. Combined effect of viscosity variation and non-Newtonian Rabinowitsch fluid in wide parallel rectangular-porous plate with squeeze-film characteristics. *Meccanica* **54**(15):2399–2409, 2019. https://doi.org/10.1007/s11012-019-01092-2

[17] P. S. Rao, A. Kumar Rahul. Effect of viscosity variation on non-Newtonian lubrication of squeeze film conical bearing having porous wall operating with Rabinowitsch fluid model. *Proceedings of the Institution of Mechanical Engineers, Part C: Journal of Mechanical Engineering Science* **233**(7):2538–2551, 2019. https://doi.org/10.1177/0954406218790

[18] A. K. Rahul, M. K. Singh, S. Saha. Squeeze film lubrication analysis and optimization of porous annular disk with viscosity variation of non-Newtonian fluid: Rabinowitsch fluid model. *Tribology International* **179**:108060, 2023. https://doi.org/10.1016/j.triboint.2022.108060

[19] H. Christensen. Stochastic models for hydrodynamic lubrication of rough surfaces. *Proceedings of the institution of mechanical engineers* **184**(1):1013–1026, 1969. https://doi.org/10.1243/PIME_PROC_1969_184_074_02

[20] H. Christensen. Some aspects of the functional influence of surface roughness in lubrication. *Wear* **17**(2):149–162, 1971. https://doi.org/10.1016/0043-1648(71)90025-1

[21] S. Alla Baksh, H. Bannihalli Naganagowda. Study of surface roughness with MHD and couple stress fluid on porous curved annular plates **62**(6):574–588, 2022. https://doi.org/10.14311/AP.2022.62.0574

[22] V. D'Agostino, A. Ruggiero, A. Senatore. Unsteady oil film forces in porous bearings: analysis of permeability effect on the rotor linear stability. *Meccanica* **44**(2):207–214, 2009. https://doi.org/10.1007/s11012-008-9180-0

[23] Y. D. Vashi, R. M. Patel, G. B. Deheri. Neuringer-Roseinweig model based longitudinally rough porous circular stepped plates in the existence of couple stress. *Acta Polytechnica* **60**(3):259–267, 2020. https://doi.org/10.14311/AP.2020.60.0259

[24] A. Siddangouda, T. Biradar, N. Naduvinamani. Combined effects of surface roughness and viscosity variation due to additives on long journal bearing. *Tribology-Materials, Surfaces & Interfaces* **7**(1):21–35, 2013. https://doi.org/10.1179/1751584X13Y.0000000024

[25] M. M. Munshi, A. R. Patel, G. B. Deheri. A study of ferrofluid lubrication based rough sine film slider bearing with assorted porous structure. *Acta Polytechnica* **59**(2):144–152, 2019. https://doi.org/10.14311/AP.2019.59.0144

[26] M. Shimpi, G. Deheri. Magnetic fluid based squeeze film in rough rotating curved porous annular plates: Deformation effect. *International Journal of Mathematical and Computational Sciences* **7**(8):1370–1380, 2013. https://doi.org/10.1155/2012/148281

[27] S. Patel, G. Deheri, J. Patel. Ferrofluid lubrication of a rough porous hyperbolic slider bearing with slip velocity. *Tribology in Industry* **36**(3):259–268, 2014.

[28] J. Patel, G. Deheri. Combined effect of slip velocity and roughness on the Jenkins model based ferrofluid lubrication of a curved rough annular squeeze film. *Journal of Applied Fluid Mechanics* **9**(2):855–865, 2016. https://doi.org/10.18869/acadpub.jafm.68.225.24447

[29] Y. D. Vashi, R. M. Patel, G. B. Deheri. Neuringer-Roseinweig model based longitudinally rough porous circular stepped plates in the existence of couple stress. *Acta Polytechnica* **60**(3):259–267, 2020. https://doi.org/10.14311/AP.2020.60.0259

[30] N. C. Patel, J. R. Patel, G. Deheri. An effect of a porous structure, slip velocity and Rosensweig's viscosity on the ferrofluid based squeeze film in porous curved annular plates. *Journal of Nanofluids* **12**(2):498–505, 2023. https://doi.org/10.1166/jon.2023.1906

[31] P. S. Rao, A. K. Rahul. Pressure generation in rough conical bearing using non-Newtonian Rabinowitsch fluid with variable viscosity. *Industrial Lubrication and Tribology* **71**(3):357–365, 2019. https://doi.org/10.1108/ILT-01-2018-0035

[32] A. Walicka, E. Walicki, P. Jurczak, J. Falicki. Influence of wall porosity and surfaces roughness on the steady performance of an externally pressurized hydrostatic conical bearing lubricated by a Rabinowitsch fluid. *International Journal of Applied Mechanics and Engineering* **22**(3):717–737, 2017. https://doi.org/10.1515/ijame-2017-0045

[33] A. K. Rahul, P. S. Rao. Rabinowitsch fluid flow with viscosity variation: application of porous rough circular stepped plates. *Tribology International* **154**:106635, 2021. https://doi.org/10.1016/j.triboint.2020.106635

[34] A. K. Rahul, M. K. Singh, S. Paul, et al. Performance analysis of annular disks with non-Newtonian Rabinowitsch fluid model: Influence of squeeze film pressure, surface roughness, porosity and viscosity variation. *International Journal of Modern Physics B* p. 2450268, 2023. [Online Ready]. https://doi.org/10.1142/S0217979224502680